WPMAT-PR(18) 20928

J Schmitz et al.

Influence of Cr-Diffusion during Plasma Exposure of WCrY Smart Alloys and Implications for the Usage as First Wall Armour Material

Preprint of Paper to be submitted for publication in
Nuclear Fusion

This work has been carried out within the framework of the EUROfusion Consortium and has received funding from the Euratom research and training programme 2014-2018 under grant agreement No 633053. The views and opinions expressed herein do not necessarily reflect those of the European Commission.

Influence of Cr-Diffusion during Plasma Exposure of WCrY Smart Alloys and Implications for the Usage as First Wall Armour Material

Janina Schmitz*[1,2], Andreas Mutzke[3], Andrey Litnovsky[1], Felix Klein[1], Xiao Yue Tan[1,4], Tobias Wegener[1], Petra Hansen[1], Alina Eksaeva[1], Marcin Rasinski[1], Jesus Gonzalez-Julian[1], Martin Bram[1], Jan Willem Coenen[1] and Christian Linsmeier[1]

[1]Forschungszentrum Jülich GmbH, Institut für Energie- und Klimaforschung, 52425 Jülich, Germany
[2]Department of Applied Physics, Ghent University, 9000 Ghent, Belgium
[3]Max-Planck-Institut für Plasmaphysik, 17491 Greifswald, Germany
[4]School of Materials Science and Engineering, Hefei University of Technology, Hefei 230009, China

July 25, 2018

Abstract

WCrY Smart Alloys are developed as first wall material of future fusion devices such as DEMO. They aim at behaving like pure W during plasma operation due to depletion of the alloying elements Cr and Y. Cr-diffusion towards the surface caused by plasma-induced Cr concentration gradients leads to enhanced erosion. In this paper the exposure of WCrY and W samples to 220 eV pure D plasma is simulated using the dynamic version of SDTrimSP. Cr-diffusion is included into the calculations. Simulation results are compared to experimental results. At sample temperatures of more than 600 °C and sputtering of W by D plus residual oxygen in the plasma ion flux, the Cr-transport to the surface suppresses W enrichment and Cr depletion. Within the model approximations and taking into account residual oxygen and D retention besides Cr-diffusion, a diffusion coefficient for Cr in WCrY of the order of $1 * 10^{-17}$ m^2/s *is determined. With respect to expected first wall conditions for DEMO, the suitability of WCrY as first wall armour, considering especially Cr-diffusion, is discussed.*

Keywords— smart alloys, plasma-wall-interaction, plasma ion irradiation, DEMO, modelling, diffusion, SDTrimSP

I. Introduction

Few materials are suitable for plasma-facing components (PFCs) of future fusion devices as there are many requirements to fulfill (see e.g. [1]). The armour material has to withstand e.g. high heat loads in the range of MWm^{-2} and simultaneously show only minor activation during neutron irradiation. Tungsten (W) currently is the preferred first wall material for next step fusion devices such as the demonstration power plant DEMO.
Advantages of W are a very high melting point of more than 3300 °C, low tritium retention and low erosion yields as well as low activation by neutrons [2]. Yet, there are also some drawbacks regarding the usage of pure W: besides its inherent brittleness at room temperature, W oxidises rapidly at temperatures of 1000 °C or more when coming into contact with oxygen (O). During a Loss-Of-Coolant-Accident (LOCA) with additional air ingress the cooling system fails. W oxidises and, having been activated by neutron irradiation during preceding plasma operation, forms radioactive WO_3. Due to nuclear decay heat wall temperatures rise to above 1000 °C to 1200 °C for several months [3], leading to the mobilisa-

*corresponding author, jan.schmitz@fz-juelich.de

tion of WO_3 and thus radioactive material into the environment. This is a severe safety hazard and has to be prevented to build safe fusion reactors.
Smart W-based alloys shall be used as first wall material in DEMO and aim to suppress the oxidation of W during LOCA. In that way only negligible amounts of radioactive material are mobilised and consequently released. These alloys contain, besides W, mainly chromium (Cr) and also small amounts of yttrium (Y). Their smartness consists in their ability to adapt to two kind of reactor scenarios: during regular plasma operation the lighter alloying elements Cr and Y are depleted towards the surface due to preferential sputtering, leaving the plasma facing a pure W surface. In that way the material benefits from the low erosion yields of W. In case of LOCA and in oxygen-containing atmosphere, the alloying elements remaining in the bulk material diffuse towards the alloy's surface. A protective oxide scale evolves on top of the alloy surface and hence the formation of WO_3 is suppressed. For the reported WCrY alloys Cr acts as the passivating element. It forms a protective Cr_2O_3 layer on top of the alloy's surface. Y serves as an active element. It is expected to facilitate Cr transport towards the surface, allowing for a more effective passivation and improved stability of the ternary system [4].
Optimum alloy composition in terms of oxidation behaviour was found to be W-11.4wt%Cr-0.6wt%Y[1] [4]. Bulk samples with this composition have been produced using Field-Assisted Sintering Technology (FAST) [5] at Forschungszentrum Jülich (FZJ). These WCrY-systems demonstrated a significant oxidation suppression of more than five orders of magnitude in comparison to pure W samples [6]. The first plasma exposure of WCrY smart alloys took place in 2017. WCrY and W samples were simultaneously exposed under steady state deuterium (D) plasma in the linear plasma device PSI-2. Whereas the exposure at an ion energy of 120 eV resulted in significant W enrichment accompanied by depletion of Cr and Y towards the surface, no significant W-enriched layer could be detected for an exposure at 220 eV. Experiments and results are described in detail in [7].
To evaluate the plasma performance of the smart alloys, possible plasma conditions at the first wall blanket modules of future fusion devices have to be examined and approximated: exact plasma parameters and thus conditions for DEMO have not been fixed yet. Still it is important to already now develop material concepts for the presumable DEMO requirements, which will differ from those for ITER [8]. The European DEMO design described in [9] is assumed to operate in H-mode with mitigated ELMs. For steady-state operation a peak heat flux of maximum 1 MWm^{-2} is assumed. Assuming a first wall armour thickness of 3 mm W on top of the structural material EUROFER-97 [8] (reduced activation ferritic martensitic steel) with a temperature limit of 550 °C [8] and further a thermal conductivity of about $1 * 10^2$ $Wm^{-1}K^{-1}$, first wall temperatures should not largely exceed 600 °C.
Besides heat loads, particle loads of different origin strike the wall. A critical criterion for the lifetime of wall components is sputtering of the material due to particle loads: plasma ions may be accelerated to energies exceeding the sputter thresholds, additional erosion is caused by charge exchange (CX) neutrals. In future fusion devices the erosion due to energetic neutrals is assumed to be of the same order of magnitude as for ions [10], in some DEMO wall areas their contribution even dominates [11]. Especially due to increasing the distance between separatrix and wall, the gap size [12], for DEMO the plasma close to the wall will be colder and thus ions hitting the wall will be less energetic. In [12] it is stated that the gap size was identified as the most promising control parameter for wall protection. Further, the perpendicular flux dominates the damage of the main chamber first wall. Neutrals, not being subject to electromagnetic forces on their path, possess energies up to several hundred eV when impinging on the wall. Also eroded neutrals from the wall are ionised in the plasma and can get accelerated in the

[1] wt%: weight percent, elemental fraction of total weight of alloy

Debye sheath near the surface to energies exceeding the wall material's sputter thresholds [11]. In this reference it is stated that fuel ions do not contribute to wall erosion due to low enough plasma temperatures near the wall without ELMs. Still impurity ions generated by wall sputtering, He ash from the fusion reaction and seeding impurities can more effectively sputter the armour material due to higher atomic number Z as compared to that of hydrogen and thus have to be taken into account. According to [9] argon (Ar), krypton (Kr) and xenon (Xe) are foreseen as seeding species for the EU DEMO. Particularly the erosion of W generates high-Z impurities at the plasma edge. Its high radiative cooling rate especially at electron temperatures typical for the plasma core puts strict constrains on the maximum allowable W core concentration, around 10^{-5}, and therefore the sputtering rate [13]. This again stresses the importance to control sputtering of W first wall armour in future fusion devices such as DEMO.

In a fusion device particle and heat loads with different energy spectra and synergistic effects of both affect the material properties of PFCs. Focussing on the impact of energetic particle bombardment on smart alloys, experiments exposing WCrY and W, for direct comparison, were carried out in the linear plasma device PSI-2 [14]. Using steady-state deuterium plasma with bias voltage applied to the target holder, energetic particle loads were simulated. In contrast to the energy distribution of the thermal ions in a fusion plasma, the ions during plasma exposure in PSI-2 were close to mono-energetic as determined by the applied bias voltage. Thus in a fusion plasma particles at the high-energy tail of the distribution may lie above the sputter threshold while the average particle energy stays below it. Temperatures in the DEMO SOL are expected to be below 100 eV [8]. In [15] ion energies of more than 100 eV and an average ion flux in the range of $1 * 10^{20}$ to $1 * 10^{22}$ ions/m^2 are ascribed to steady-state DEMO operation. For ion energies of around 100 eV in pure D no W sputtering is expected, except for the residual oxygen in the plasma (see table 3 for sputter thresholds). The design question whether high heat flux limiters will be installed still remains open for DEMO [8]. In limited configuration, e.g. during ramp-up or ramp-down of the plasma, the plasma gets closer to the wall and ion energies are elevated due to higher SOL temperatures as compared to the diverted configuration. For ITER limiter geometry strong W erosion is expected even for pure D plasmas from DIVIMP simulations [13]. The sputter threshold for D on W is around 220 eV [16]. With the aim of investigating plasma-induced changes in case of W sputtering by not only residual O, an ion energy of 220 eV was chosen. In PSI-2 experiments the plasma flux, which hits the target at normal incidence, additionally leads to heating of the samples. According to [12] the impinging perpendicular flux plays the dominating role for the global average damage of the main chamber first wall.

The importance of preferential sputtering and resulting depletion of alloying elements accompanied by enrichment of W calls for encompassing understanding of sputtering processes at the alloy's surface. Additionally, Cr-diffusion, which is of paramount importance for the alloy's oxidation performance, can influence the alloy's erosion yield. For this reason modelling the plasma impact onto the alloy's composition using the Monte-Carlo code SDTrimSP ([17]) with inclusion of thermal diffusion was carried out. The code makes use of the Binary-Collision-Approximation (BCA) to simulate ion irradiation of amorphous targets. The underlying physics are described in [16]. In the dynamic version a one-dimensional target made up of dynamically thickening or shrinking layers is employed. The ion projectiles subsequently shot into the target create recoils and eventually sputtering of subsurface atomic layers if the surface binding energy is overcome. Gradients of elemental distribution are induced in case of preferential sputtering. With diffusion added to the model, the depleted element is transported towards the surface to counteract the build-up of the gradients. Owing to the usage of the dynamic version we are able to look into the evolution of the alloy's

composition rather than merely obtaining the final state from experimental analysis.
In this paper experimental results of the D plasma exposure at ion energies of 220 eV are compared to modelling results: first the smart alloy concept and the prerequisites for DEMO first wall material to motivate the plasma experiments are introduced. While the second section is devoted to a short overview of the experimental setup and analytic techniques, the third section describes in detail the relevant experimental results. Consequently, in the fourth chapter a description of the used SDTrimSP Model is given, followed by the results of the calculations in chapter five. The sixth chapter then discusses both experimental and model results comprising limitations of the applied model and possible extensions as well as relevance for usage of smart alloys in DEMO. In the end a short summary is given alongside with an outlook on future research.

II. Experimental Setup and Analytic Techniques

i. Sample Production and Preparation

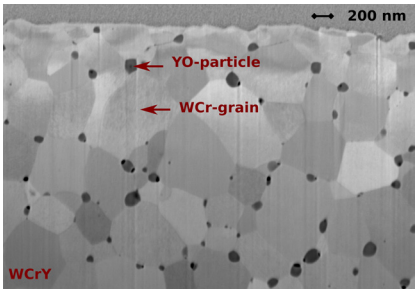

Figure 1: FIB cut (orthogonal to surface) of a WCrY sample. The microstructure is characterised by YO-particles located at the grain boundaries of a solid solution of WCr grains.

Bulk WCrY samples are produced by FAST with the optimum alloy composition ([4, 6]). In figure 1 one can see the microstructure obtained by means of the FAST-process from the cut orthogonal to the sample surface. YO-particles (size of the order of tens of nm) are finely dispersed in between a solid solution of W-Cr grains (size of the order of hundreds of nm). The yttria is located mainly at the grain boundaries. A more detailed description of the grain structure and the sample production process can be found in [6]. Following the production of the ingots, samples are then cut by means of spark erosion to fit the PSI-2 mask geometry. The plasma-facing surface of all WCrY and pure reference W samples spans over 1 cm x 1 cm.
For removing remnants from wire erosion the two WCrY samples, WCrY1 and WCrY2, and the two W samples, W1 and W2, are manually ground. The surface roughness of the finished samples amounts to approximately 30 nm for all samples.

ii. Experiment and Analysis Methods

Experimental parameters are given in table 1.

plasma	ion energy [eV]	ion flux [ions/m^{2}s]	ion fluence [ions/m^2]	sample temperature [°C]
D[a]	220	$5.5 * 10^{21}$	$1 * 10^{26}$	620-650

Table 1: Experimental plasma parameters in PSI-2

[a] plus residual O content ($<$ 1 % of ion flux)

Due to target biasing of about 250 V and a plasma potential of 30 eV, measured by a Langmuir probe, the ion energy is mono-energetic with 220 eV. The plasma flux at normal incidence leads to heating of the samples to temperatures of around 620 to 650 °C.
For the purpose of comparing the experimental results to the SDTrimSP model, we focus on the results for the samples' weight loss, Δm, the surface recession d_e and surface morphology as well as plasma-induced changes of the (sub-surface) elemental composition. Analytical methods are described in [7].

III. Experimental Results

i. Results of Plasma Exposure

Weight and volumetric loss as a measure for the erosion yield of pure W and WCrY smart alloy samples exposed in PSI-2 are displayed in figure 2. Whereas

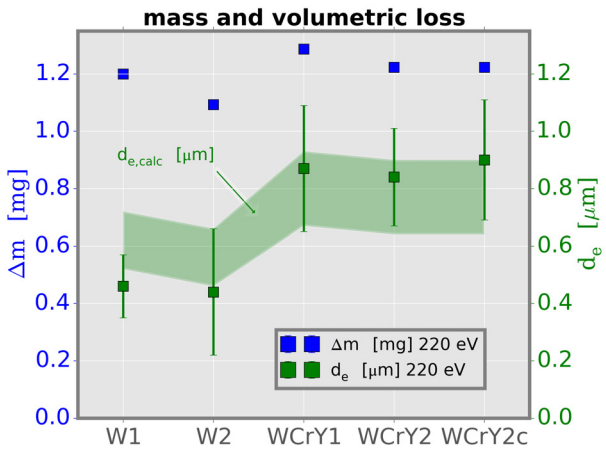

Figure 2: Comparison of mass loss Δm and volumetric loss d_e for pure W and WCrY samples. WCrY2c depicts the measurement of volumetric loss (surface recession) for a FIB crater at the corner of WCrY2. All other craters were cut in the sample centre.

the mass loss Δm is very similar for all samples, around 1.1 mg for W to 1.2 mg for WCrY, the volumetric loss is nearly doubled for the WCrY alloys. This result indicates preferential sputtering of the lighter alloying elements Cr and Y. The green ribbon ($d_{e,calc}$) displays the expected volumetric loss, which is calculated from the mass loss and under the assumption of homogeneous erosion across the sample surface. As the measured values for d_e agree within error bars with $d_{e,calc}$ the assumption of homogeneous erosion is validated. A further support for this are the alike local erosion values for the FIB craters in the middle and corner of WCrY2. By comparing weight and volumetric loss of the smart alloy samples the density of the eroded material ρ_e is determined:

$$\rho_e = m_{loss}/V_{loss} \approx 1200\ \mu g/(850\ nm \cdot 1\ cm^2)$$
$$\approx 14.1\ g/cm^3$$

Taking the initial alloy composition to be W-11.4wt%Cr-0.6wt%Y, which is equal to 67.9at%W-31.1at%Cr-1at%Y[2], the initial theoretical density of the smart alloy is $\rho_i = 15.9\ g/cm^3$. Measurements according to the Archimedes principle confirmed an initial density of more than 98 %, which corresponds to 15.6 g/cm^3, of the theoretical density for the two smart alloy samples WCrY1 and WCrY2. Since the value of ρ_e is smaller than ρ_i, one can conclude that lighter elements were eroded proportionally more during plasma exposure. The elemental composition is homogeneous before plasma exposure (see also Secondary Ion Mass Spectrometry (SIMS) analysis results in [7]). Already from this result it becomes evident that lighter elements must have been transported towards the surface to be continuously sputtered and lower the density of the eroded material. Since an ion energy of 220 eV is about the

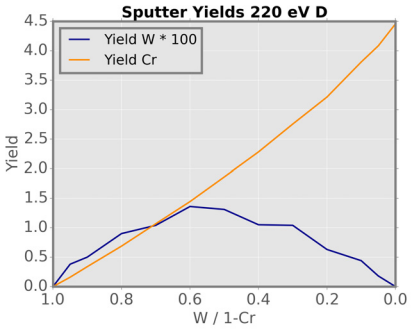

Figure 3: Calculated sputter yields of D on a WCr target with a composition varying from pure W (1W / 0Cr) to pure Cr (0W / 1Cr)

threshold for physical sputtering of W by D ions (see [18] and table 3), the small amounts of residual oxygen in the plasma dominate the material's erosion. Further, Cr atoms existent in the vicinity of W atoms beneath the surface lead to enhanced W sputtering: with an intermediate Cr-W collision instead of the direct energy transfer from D to

[2]at%: atomic percent, elemental fraction of total atomic composition of alloy

W the energy transfer is augmented see [7]. This is shown in figure 3. Hence not only the lighter alloying elements but also the heavy element W gets sputtered by D and O in this experiment for both the pure W and WCrY samples.

In figure 4 one can see the depth-resolved signals

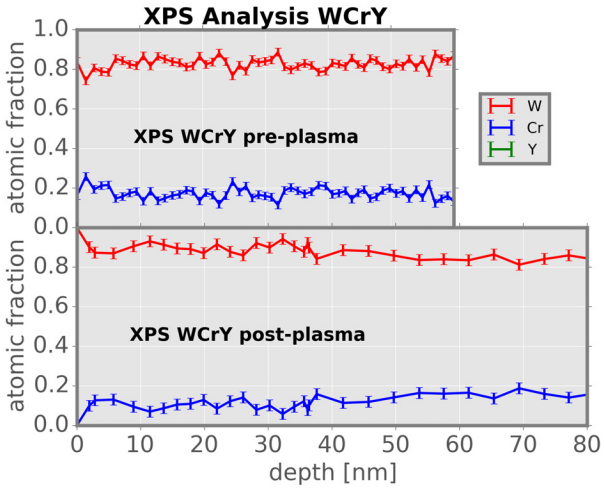

Figure 4: XPS sputter-analysis for WCrY smart alloy a) before and b) after exposure to 220 eV pure D plasma

for W and Cr obtained by XPS. The W- and Cr-concentrations are normalised to yield a value of 1 when summed over. Whereas the W- and Cr-content for the non-exposed WCrY sample (4 a) are homogeneous along the sample depth, the W-signal of the exposed sample (4 b) shows a slight ascent towards the surface, indicating a modest W enrichment.

At a vacuum pressure of $10^{-8} - 10^{-9}$ mbar in the XPS device the oxidised surface layer of the material is removed after the first Ar-sputter process (second data point). The formation of new oxide monolayers takes at least several minutes at this low pressures and does not have time to occur in an interval of tens of seconds between sputtering processes. The Y-signal was below the detection limit and hence was measured to be zero at all times. As the concentration of Y within the alloy amounts to only 1 at% it plays a minor role in the erosion behaviour of the alloy system and its effect is less significant as against the effects of Cr and W.

ii. Vacuum Heating and XPS-Analysis

During plasma exposure in PSI-2 samples are subject to ion bombardment and heat deposition at the same time. The XPS-device allows to heat samples to high temperatures under ultra-high-vacuum (UHV) conditions at a pressure of $10^{-8} - 10^{-9}$ mbar. This provides the possibility to distinguish diffusion effects caused by elevated temperatures from those caused by ion bombardment.

The surface composition of one piece of sample WCrY1, was first ground according to the normal sample preparation procedure (see section II) (figure 5 a), and heated to 627 °C for 1 hour under UHV conditions (figure 5 b). Then the surface was examined by SEM, put again into the XPS device, sputtered by Ar and heated again to 627 °C for 3 hours (figure 5 c). One should note that the scratches from grinding are not uniformly distributed across the sample surface and the SEM pictures are not taken at exactly the same position before and after the XPS treatments.

When examining the sample's surface after the first heat treatment (figure 5 b) using the electron microscope of the SEM-FIB device, no visible indications for Cr-diffusion, such as increased Cr-concentration of the surface, were detected, the surface morphology looks like the one obtained after grinding (figure 5 a). The characteristic surface features in figure 5 a, elongated scratches, stem from the grinding process and are not altered by the heating process to 627 °C. The sample's surface composition was then measured by XPS with preceding Ar-sputtering and heated again to 627 °C for 3 h and measured afterwards without repeating the Ar-sputtering. The 5 keV Ar-sputtering is used for removing residual oxygen and impurities (as present from values in table 2 a) from the surface. This process leads not only to a removal of an approximately 3 nm thick surface layer, but also to a characteristic surface morphology

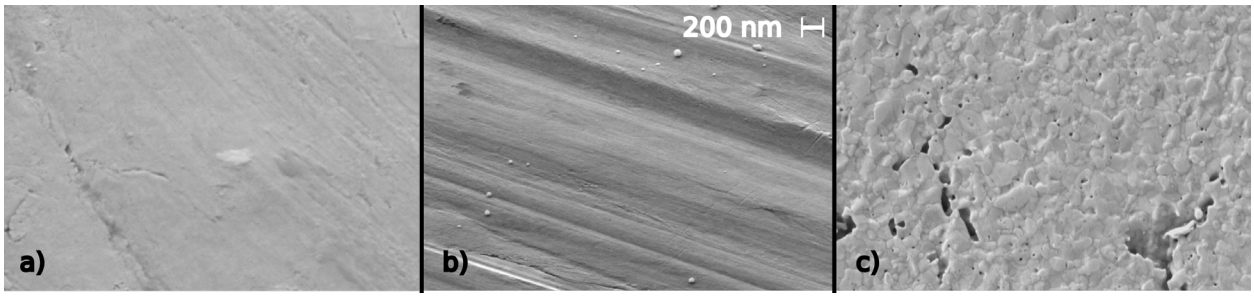

Figure 5: SEM pictures of the surface of a piece of WCrY1 a) after grinding and before the XPS-heating treatment, b) after heating to 627 °C for 1 h in UHV conditions, c) after Ar-sputtering and heating to 627 °C for 3 h in UHV conditions.

of small holes and elongated craters along the grain boundaries due to preferential sputtering of lighter elements. This becomes evident in figure 5 c. As described in section II the microstructure features YO-particles located at grain boundaries. The small black holes on the Ar-sputtered surface are assumed to be locations of sputtered YO-particles of the size of the order of tens of nm. Removing 3 nm from the surface corresponds to several monolayers of pure W with a monolayer thickness of about 0.3 nm. Not only is Y lighter in comparison to W and hence sputtered more easily, also the fact that it is present in the form of yttria and hence oxidised increases its sputter yield. From the purely visual aspect the obtained surface morphology looks similar to the one obtained after plasma exposure of smart alloys as presented in [7].

When comparing the elemental surface composition from before and after heating to 627 °C for 3 h (table 2 b and c) a slight increase in the Cr-content and pronounced increase in O-content of the subsurface layer is evident. After preferential sputtering has altered the initial surface composition, some Cr diffuses towards the surface. Despite the UHV conditions of the XPS-device, Cr_2O_3 is formed at the surface. The 17.9 % Cr fraction is composed of 28 % Cr_2O_3 and 72 % elemental Cr.

	W [at%]	Cr [at%]	Y [at%]	other elements [at%]
a)	13.7	2.9	0.7	32.3 (O), 25.0 (C), 0.5 (Mo), 24.9 (F)
b)	82.8	16.3	0.0	0.9 (Mo)
c)	68.8	17.9	0.0	15.5 (O), 1.0 (Mo)

Table 2: XPS-analysis of a piece of WCrY1 a) before heating and without Ar-sputtering, b) after heating for 1 h to 627 °C and subsequent Ar-sputtering and c) after heating for 3 h to 627 °C

In conclusion XPS-analysis indicates only weak diffusion of Cr towards the surface and no changes in the microstructure at temperatures of 627 °C, approximately the temperature of the samples during plasma exposure. Whereas even in UHV conditions Cr is oxidised on the surface, no W-oxides could be detected. For the sample temperatures of close to 627 °C during plasma exposure this means that without preferential sputtering no significant diffusion of Cr is expected. Since Cr oxidises already at very low vacuum pressures and there is some residual oxygen present in the plasma ion flux onto the target, potentially also lower erosion yields of Cr-oxides as against Cr adds to the effect of preferential sputtering of the lighter elements.

IV. Model Description

In order to model the erosion of the smart alloy system during plasma exposure the Monte-Carlo code SDTrimSP is employed. Since a one-dimensional target model is used, we do not reproduce the specific microstructure but rather assume a homogeneous distribution of W, Cr and Y with a composition of 67.9at%W-31.1at%Cr-1at%Y and an amorphous tar-

get structure. Within the herein applied dynamic version of the code the target, which is initially subdivided into equidistant slabs of the same composition, is updated after a certain number of projectile ions has been calculated. After each such fluence step the number of the respective atomic species in each slab and hence the concentrations of the elements are changed. This, in turn, causes a change in the atomic density and finally an increase or decrease of the slab thickness Δx_i (figure 6), here initially 2.5 Å. Summing over the changes in thickness of all slabs leads to growing of the target if more atoms are deposited than sputtered. If erosion dominates the summation results in shrinkage which is quantified by the surface receding over a certain distance. For the calculations normal incidence of the bombarding ions is assumed. The surface roughness of about 30 nm cannot be reproduced with the one-dimensional model. This should not have a large impact on the erosion results for the case of normal incidence irradiation, but may have an impact on the first few nm of the profiles obtained by surface analysis.

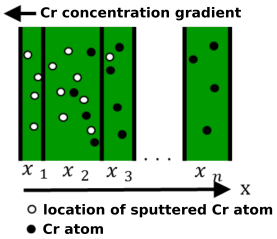

Figure 6: Scetch of the dynamic target model with neighbouring slabs (surface layers) x_i and preferential sputtering of Cr-atoms giving rise to Cr-diffusion towards the surface

i. Inclusion of Diffusion into the Model

Since SDTrimSP 5.07 [17] thermal diffusion between adjacent target layers can be included into the model if the temperature-dependent diffusion coefficients are known. Generally, concentration gradients within a material, see equation 1 depicting the evolution of the element-specific (i) concentration c at position x, lead to diffusion of elements to counteract the build-up of gradients. Diffusion increases exponentially with temperature (see equation 2). Still for triggering the process a difference in atomic densities of a certain element between adjacent layers must exist. In the dynamic target model diffusive transport across the surface boundary by diffusion is set to be zero. However, if atoms of the first layers get sputtered by plasma ions, the induced concentration gradient between two target layers initiates diffusion. Without taking diffusion into account the amount of eroded material depends on the accumulated fluence and is independent of the rate at which the fluence is accumulated, i.e. the ion flux. In case thermal diffusion plays a role the flux, the number of ions arriving at the target per second, is used to introduce a time dependence since the diffusion coefficient (see equation 2) is given in m^2/s. The time for a fluence step results from equation 3, this time is then used for the diffusion calculation. Calculated recoils result in changes of the concentrations c of the elements i within each slab x_i. Based on this concentration change the slab-specific diffusion coefficient $\eta(x,i)$ (see equation 4) is calculated. This is done by summing over the concentrations and diffusion coefficients of element i within material j for all elements j (see equation 4).

$$\frac{\partial c(i)}{\partial t} = -\frac{\partial(\eta(x,i)\cdot\frac{\partial c(x,i)}{\partial x})}{\partial x} \tag{1}$$

$$D(i,j) = D_0(i,j)\cdot\exp(-\frac{Q_a(i,j)}{k_B T}) \tag{2}$$

$$\Delta t = \frac{\Delta\text{fluence } [m^{-2}]}{\text{flux } [m^{-2}s^{-1}]} \tag{3}$$

$$\eta(x,i) = \sum^{j} c(x,j)\cdot D(i,j) \tag{4}$$

According to the Arrhenius formula in equation 2 two parameters have to be specified to assign a diffusion coefficient D(i, j) for element i in element j. In order to vary just this parameter for the simulations we do not specify the activation energy Q_a (see [19] for detailed explanation). Therefore, the simulations are just valid for the sample temperature present in the experiment. In that way different simulations for a varying value of $D_0(i,j)$ can be performed at

the sample temperature as given in the experiment. For the simple physical sputtering process, temperature is not taken into account within the BCA. The implementation of the used algorithm to solve the diffusion equation and further details are described in detail in [20].

V. Calculations

	bombarding ion species		
target	**D**	**O**	**Ar**
W	220	45	35
Cr	35	20	20
Y	60	15	20

Table 3: Thresholds [eV] for pure elements W, Cr and Y sputtered by D, O and Ar as calculated with SDTrimSP using surface binding energies of 8.79 eV, 4.10 eV and 4.36 eV for W, Cr and Y, respectively at normal incidence.

Sputter Yields for the pure elements W, Cr and Y calculated with SDTrimSP in static mode are shown in table 3. The thresholds for W and Cr are about 220 eV and 35 eV, respectively and are approximately in agreement with the threshold values as presented in [21], 216 eV for W and 34 eV for Cr. For O sputtering thresholds are considerably lower according to SDTrimSP Results in the table: 45 eV for W and 20 eV for Cr. Consequently it can be expected that already small amounts of O in the target ion flux have a large impact on the material's erosion.
With $1 * 10^{26}$ ions/m^2 the experimental fluence corresponds to more than one day of continuous DEMO operation, assuming a perpendicular ion flux of the order of $1 * 10^{21}$ ions/m^{2}s [12]. It is expected that lighter alloyed elements are preferentially sputtered, which leads to a continuous change of the surface stoichiometry during ion irradiation until a steady state is reached [21]. For this state the ratio of the sputtering yields is stoichiometric [22]. For dynamical SDTrimSP runs this means that after a certain fluence partial sputter yields converge as does the fractional target composition. From this fluence the results can thus be extrapolated to larger fluencies. The simulations calculate 10 % of the experimental fluence, which is $(1 * 10^{26} \cdot 0.1 =)\ 1 * 10^{25}$ (ions/m^2), assuming steady state has approximately been reached at this point. The assumption is supported by the asymptotic trend of the partial sputter yields (see e.g. figure 8c). In that way the computation time can be reduced considerably. The last 10 values of this simulation are then used to linearly extrapolate the surface recession: the slope of a line intersecting this last 10 values is assumed to be constant till 100 % of the experimental fluence is reached. Different from the surface recession, the mass loss is indirectly obtained from the simulation output by integration of the partial yield curves as shown in figure 8c. Mass loss values were extrapolated using the partial sputter yields of W, Cr and Y at the last fluence step. One simulation run, indicated by triangles in 8a and shown in figure 7c, was extended to match the experimental fluence to evaluate the matching of calculation and extrapolation.
To tune the model parameters experimental values are used for benchmarking: local erosion obtained by FIB (see section III) is taken to be around 450 nm for pure W and 850 nm for WCrY. Weight loss reference values for W and WCrY are 1.1 mg and 1.2 mg, respectively.

The weight and volume loss of the pure W samples exposed alongside with the WCrY samples are utilised to validate the simulation results. Neither preferential sputtering nor diffusion have to be considered for the erosion yield of pure W samples. It should be kept in mind that we obtain the net erosion of the plasma-exposed samples, effects due to e.g. redeposition and thus the gross erosion cannot be evaluated.
Given that the employed model is only one-dimensional and does not comprise other possible phenomena such as surface segregation, redeposition or self-sputtering, simulations aim at qualitatively understanding the interaction of sputtering and diffusion processes. Obtained diffusion coeffi-

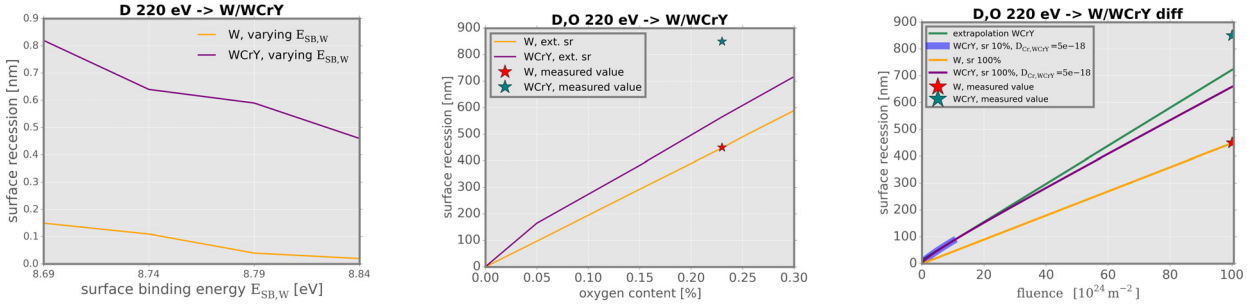

a) b) c)

Figure 7: SDTrimSP calculated surface recessions [nm] under D, O 220 eV ion bombardment: a) extrapolated values for pure W and WCrY with pure D ion irradiation varying the W surface binding energy $E_{SB,W}$. b) extrapolated values for pure W and WCrY with mixed D, O ion irradiation with variation of the oxygen content O. c) mixed D, O ion irradiation (0.23 % O) of pure W and WCrY ($D_{Cr,WCrY} = 5 * 10^{-18}$ m^2/s) calculated for the experimental fluence of $1 * 10^{26}$ ions/m^2 (W and WCrY 100 %) and $1 * 10^{25}$ ions/m^2 (WCrY 10 %).

cients rather give an indication how strong the overall Cr-transport towards the surface during plasma exposure is than being an exact measure for purely thermal Cr-diffusion. Both the measured mass loss and even more the surface recession are subject to measurement uncertainties (see figure 2), which is considered for determining the model parameters.
In the following the effect of the different model parameters, D ion irradiation, surface binding energies of W and Cr, oxygen plasma content, Cr-diffusion and D retention is presented according to their order of implementation. Subsequently, further factors which have not been taken into account are looked upon.

i. Pure D Irradiation

At first simulations using solely D ions were carried out. Results for W and WCrY are displayed in figure 7a. Commonly, for BCA models the heat of sublimation energy is used as an approximation for the surface binding energy E_{SB}, as the actual E_{SB} values are unknown [23]. This is the energy that is needed to overcome for a target surface atom to get sputtered. For tungsten the default value in SDTrimSP tables is 8.79 eV. The calculated surface recessions extrapolated to 100 % experimental fluence for W are far below the experimental value of 450 nm at a surface binding energy of W, $E_{SB,W}$, initially set to 8.79 eV. $E_{SB,W}$ was thus varied from 8.69 eV to 8.84 eV. For all these runs only very few atoms are eroded from the sample, for W the expected surface recession amounts to only below 1 nm compared to about 450 nm as reported from experiment. Likewise, the calculations for WCrY with varying values of the W surface binding energy result in very low surface recession values. Consequently, other factors influencing the sputter yield during exposure in PSI-2 have to be considered.

ii. Mixed D, O Irradiation

Especially at deuterium ion energies close to or below the threshold for physical sputtering, the effect of sputtering due to impurity oxygen becomes important [24]. A lower surface binding energy or a higher oxygen content in the plasma lead to enhanced sputtering. It becomes evident from graph 7a that varying only the W surface binding energy will not yield the expected recession. Thus the plasma oxygen content was varied in a next step. This value likely amounts to a few tenths of one percent in PSI-2. Here we want to stress again that possible effects of sputtered material deposition was not taken

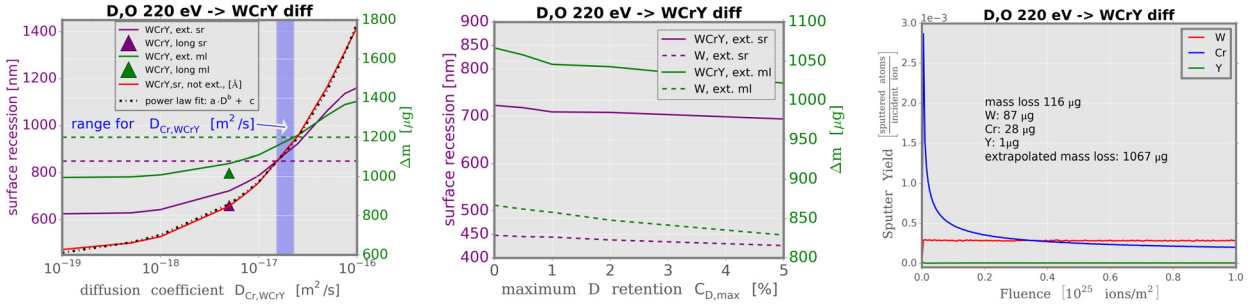

a) b) c)

Figure 8: SDTrimSP calculations under D, O (0.23 % O) 220 eV ion bombardment including diffusion: extrapolated (ext.) surface recession (sr) and mass loss (ml) with a) varying diffusion coefficient, power law fit of not extrapolated surface recession values (in red) with a = $4.6 * 10^{10}$, b = 0.5, c = 564.5. b) with varying maximum retained D fraction $C_{D,max}$ [% of the target atomic target density] at a fluence of $1 * 10^{25}$ ions/m^2 and oxygen content of 0.23 %. c) simulated partial sputter yields of W, Cr and Y for WCrY with the diffusion coefficient of Cr in WCrY fixed to $D_{Cr,WCrY} = 5 * 10^{-18}$ m^2/s. By integration of the partial yield curves the mass losses per element are obtained. The triangles in figure a represent the non-extrapolated data points of a simulation run extended to 100 % experimental fluence with 0.23 % O and $D_{Cr,WCrY} = 5 * 10^{-18}$ m^2/s without D retention (see figure 7c). The green and purple dashed lines represent the experimentally found values of around 1200 μg mass loss and 850 nm surface recession, respectively.

into account. The actual oxygen content of the ion flux may thus be higher, meaning material was sputtered and deposited again and hence does not count towards mass loss. In figure 7b recession versus varying oxygen content is displayed for both pure W and WCrY at $E_{SB,W}$ fixed to 8.79 eV. Since experimental surface recession of pure W (450 nm) agreed assuming a plasma composition of 99.73 % D and 0.23 % O, this composition was used for further calculations. Whereas with including oxygen-induced erosion the experimentally obtained surface recession of pure W can be rendered, the WCrY surface recession of about 565 nm is far below the experimental value. Also with simultaneously varying surface binding energies at a fixed oxygen content of 0.23 % in the D plasma, the experimental value could not be matched. For $E_{SB,W}$ ranging from 8.69 eV to 8.84 eV the difference in surface recession amounts to only about 2 nm. Since plasma conditions are approximately the same at all sample locations, another factor must be responsible for the enhanced erosion in case of the WCrY smart alloy. For this reason and based on the experimental finding of the decreased density ρ_e of the eroded alloy material (see section III), diffusion has to be included in the SDTrimSP model.

iii. Mixed D, O Irradiation including Cr-Diffusion

For the variation of the diffusion coefficient of Cr in WCrY the oxygen content of the plasma is fixed to 0.23 % and the surface binding energy of W set to 8.79 eV. Results are displayed in figure 8a. The diffusion coefficient was varied over several orders of magnitude. Surface recession values are calculated up to a fluence of $1 * 10^{25}$ ions/m^2 and then extrapolated as shown in figure 7c. The blue shaded bar indicates the range for the diffusion coefficient so that simulation results either match the experimentally found surface recession (lower bound) or the experimentally found mass loss (upper bound). The simulated data point for $D_{Cr,WCrY} = 5 * 10^{-18}$ m^2/s at the experimental fluence is indicated with triangles. For this diffusion coefficient the surface recession at 10 % of the experimental fluence is matched by the simulation results. For the extrapolated mass loss and surface recession values to match the experimental

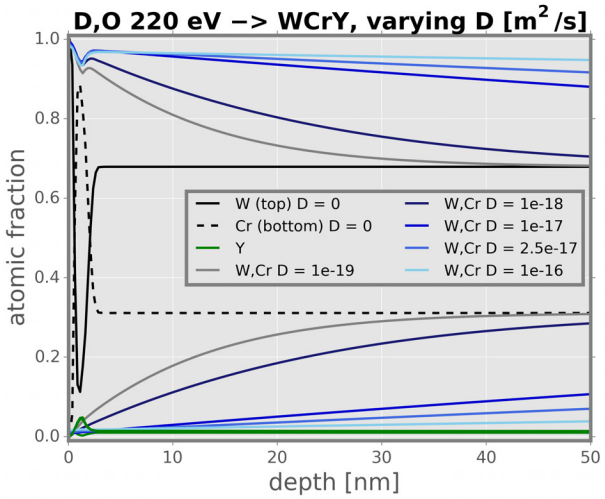

Figure 9: Target composition at last calculated fluence step ($1 * 10^{25}$ ions/m^2) for values of $D_{Cr,WCrY}$ (referred to as D in the graph) varying from 0 to $1 * 10^{-16}$ m^2/s. W and Cr profiles (at top and bottom of the graph, respectively) at a certain D-value have the same colour. Y profiles for all D-values are coloured in green.

reference values at the chosen model parameters, the diffusion coefficient has to be set to a value within the indicated range: 2 to $3 * 10^{-17}$ m^2/s. In order to compare extrapolated values directly to the simulation output, one calculation was extended for W and one for WCrY up to a fluence of $1 * 10^{26}$ ions/m^2 with $D_{Cr,WCrY}$ set to $5 * 10^{-18}$ m^2/s. Results are indicated as triangles in figure 8a and in addition displayed in figure 7c. Here the W surface recession agrees well with the experimentally found value of 450 nm. At the same time, the WCrY surface recession remains with approximately 660 nm below the reference value of 850 nm for 100 % experimental fluence as well as below the extrapolated value of 723 nm. Taking 10 % of the experimental surface recession of WCrY, 85 nm, we see that this value is met at a fluence of $1 * 10^{25}$ ions/m^2. However, since the surface recession is not strictly linear for WCrY, which is mirrored by the partial sputter yield evolution, the model results deviate for later steps. If more Cr is present at the surface, the Cr partial sputter yield is increased while W sputtering is at a low level. In this state surface recession is accelerated against states of higher W concentration at the sample surface. Again, changes in W and Cr surface binding energies play only a minor role. For $E_{SB,W}$ ranging from 8.64 eV to 8.84 eV and $E_{SB,Cr}$ ranging from 4.00 eV to 4.15 eV the differences in surface recession amount to about 2 nm and less than 0.5 nm, respectively.

In figure 8c the evolution of the partial sputter yields of W, Cr and Y is displayed. The total mass loss is the sum of the partial mass losses for W, Cr and Y. On average most of the mass loss is caused by W sputtering, whereas at the beginning of the ion irradiation Cr sputtering is predominant. Due to the small Y content in the sample, mass loss caused by Y sputtering does not play a crucial role.

Further, Y-diffusion is neglected. In the graph of figure 9, which displays the final target composition with varying Cr-diffusion coefficients, a peak in Y concentration beneath the sample surface stemming from Y recoils is visible. As a consequence of the Y surge there is a dip in W concentration at the same position. For Cr this peak is suppressed due to the Cr-mobility: without diffusion there is a shallow 2 to 3 nm wide layer where Cr peaks (dotted black line at D=0) and W enriches (solid black line at D=0). Moreover, in this figure it is apparent that by increasing $D_{Cr,WCrY}$ the change in sample composition induced by plasma sputtering extends further into the depth of the sample. Cr is transported from increasingly deeper layers to the top surface layers which are affected by erosion.

iv. Influence of D Retention

A further parameter exerting influence onto the modelled erosion behaviour for both W and WCrY is the deuterium retention during the exposure. For the considerations described in this paper we generally assume deuterium to behave like hydrogen. In [25] it is stated that the amount of hydrogen retained in W is determined by defects as hydrogen solubility is generally low in W. The grinding process described in section II creates a damaged subsur-

face layer, which could lead to enhanced D retention beneath the surface of the exposed samples. As the D ion energies are well below the threshold of 933 eV for D ions to create lattice displacements in W [26], no additional damage generation is expected during plasma exposure. Still [27] reports the generation of additional traps for deuterium below the damage threshold during exposure of W and W-Tantalum (Ta) alloys. In the same paper no difference in the amount of retained W and W-Ta was found, although [28] states that a higher intrinsic trap density in W-Ta alloys raises retention. In [7] D retention was found to be just slightly increased for WCrY, with an amount of the order of $1 * 10^{14}$ at/cm^2 ($\widehat{=}$ $1 * 10^{-5}$D/WCrY) which is why for the calculations we make the same assumptions regarding the fraction of D retention for W and WCrY. Although at the high sample temperatures of 620 to 650 °C during the exposure D gasses out easily again and is hence very low when measured after the exposure, for a moment it may be present in the target during the exposure and hence influence the sputtering behaviour.

Within the SDTrimSP model the maximum retained D fraction in at% within the sample can be chosen. In figure 8b extrapolated simulation results for surface recession and mass loss for W and WCrY are shown for different values of the maximum retained D fraction $C_{D,max}$ [%] at a fluence of $1 * 10^{25}$ ions/m^2. Calculations of lost mass are carried out according to the procedure described in 8c. The diffusion coefficient for Cr in WCrY was set to $5 * 10^{-18}$ m^2/s for these simulation runs. For higher diffusion coefficients accompanied with D retention surface recession and mass loss do not agree with experimental results. Choosing a maximum amount of retained D inside the target, outgassing of D is approximately included into the model, as surplus D atoms are ejected.

With increasing $C_{D,max}$ more D atoms are implanted and retained and the target density is reduced as the light D atoms attribute considerably more to a volume increase than to a weight increase of the target. Less W is located at the target surface leading to a reduced W sputter yield. As a result, the surface recession and more pronounced the mass loss are reduced with rising D-retention. Diffusion of D in W and WCrY is set to $D_{D,W/WCrY} = 1 * 10^{-17}$ m^2/s. To elevate the reduced W surface recession value again, the oxygen content of the plasma, which has previously been set to 0.23 % (see section ii) has to be readjusted. The measurement uncertainties of the experimental weight loss are smaller compared to the surface recession obtained by FIB. Consequently, for improving the agreement between model and experiment we look more closely on matching the mass loss values. For example, assuming a plasma composition of 99.71 % D and 0.29 % O the simulation yields a surface recession of about 533 nm for W at $C_{D,max} = 2$ % and a mass loss of 1066 µg.

v. Influence of Other Factors

In the following paragraph the influence of three further factors is outlined and weighted.

Firstly, within SDTrimSP different surface binding energy models can be used. For the presented simulation results a surface binding model with constant surface binding energies was used (see [17] model 1 for detailed description). Compared to other models with varying surface binding energies (models 2 and 3 in [17]) the difference of recession values among the models amounts to less than 1 nm for a calculated fluence of $1 * 10^{25}$ ions/m^2 and mixed D, O irradiation on WCrY including diffusion. Simulations using constant surface binding energies need slightly less computational time.

Secondly, in [29] and [30] a reduced energy threshold for oxidised W sputtered by light ions as compared to pure W, resulting from a decrease in the binding energy of tungsten oxide molecules, is reported. After heating a WCrY sample for 3 h to 900 K in the UHV conditions of the XPS device no W-oxides were found on the surface. Assuming a sputter yield of about 0.001 for D ions at approximately 200 eV on WO_3 (compared to $\sim$ 0.0001 for pure W) [29], a 1 nm thick layer of oxidised tungsten present at the start of the plasma experiment would be eroded

within seconds. Yet, as described in section ii, the formation of Cr_2O_3 was detected. In SDTrimSP only binary atom collisions are considered, so the effect of possible oxide formation is not taken into account.
Lastly, for determining the effect of self-sputtering and redeposition of W and Cr ERO modelling was performed. ERO is a 3D Monte Carlo code used for simulating transport of sputtered particles. As described in [31] there exists a version adapted to the PSI-2 geometry. Calculations employing this version and plasma parameters taken from measurements during the experiment were executed for pure W and Cr targets. Mass change by redeposition and self-sputtering for W and Cr were around 26 and 14 %, respectively. Thus by neglecting deposition especially of W and comparing the net erosion instead of gross erosion of the experimental results with the model, the plasma oxygen content may be higher than 0.3 % as described in section ii. To investigate the sputtering and deposition processes during the experiment, spectroscopy measurements to detect Cr- and W- line emission in the vicinity of the target are necessary.

VI. Discussion

During the exposure in PSI-2 the sample surface temperatures are not instantly constant at the start of the exposure. We only derive a temperature-averaged diffusion coefficient. The same is true for the impurity concentration and other plasma parameters. As the model parameters are fixed to certain values at the beginning of a simulation run, they represent the average values of possible fluctuations. Possible trace amounts of impurities, for example by using graphite foil during the FAST sample production, may alter the material's plasma behaviour such as for example D retention. Yet, the characteristics mainly determining the erosion behaviour of the smart alloys are the W distribution at the sample's surface and the Cr-transport within the material.
Concerning the general effect of the different model parameters the following conclusions can be drawn: by using the fact that, unlike a WCrY sample, the composition of a pure W sample does not change during plasma exposure, a value of for the oxygen content of the plasma, without taking into account redeposition and self-sputtering, is fixed. Comparison of experimental and simulation results for D ion irradiation on W and WCrY, including the effect of residual oxygen in the plasma (section ii), highlights the need for diffusion in the current model. An increased diffusion coefficient of Cr in WCrY causes increased (extrapolated) surface recession and mass loss (figures 7c and 8a). Fitting the curve of the surface recession versus the diffusion coefficient in figure 8a yields a square-root-dependence (b=0.5). This is the same dependence as for the diffusion length $d_l = 2 * \sqrt{Dt}$ (see [19]), the characteristic distance for the propagation of the diffusing species' concentration. Thus the thickness of the sputtered sample layer is similar to the diffusion length.
Changes in surface recession resulting from different values of the surface binding energies for W and Cr are minor. Hence, the surface binding energies exhibit only negligible influence. By considering also D retention of the samples, the plasma oxygen content needs to be elevated in the model to again match experimentally found mass loss values as described in section iv. Depending on whether one focusses closer on matching experimental results for weight loss or surface recession, the model parameters such as diffusion coefficient, oxygen content or D retention can be adjusted.
Oscillatory behaviour as described in [20] was found neither for sputter yields nor for surface concentrations. This is why the initial slab width of 2.5 Å used in the target model is assumed to be appropriate to prevent the addition of synthetic effects to the Cr-diffusion process. The sharp decrease of the Cr partial sputter yield (figure 8c) can be ascribed to a W-enriched layer at the target surface. Similar experimental findings are presented for W-enrichment in CLF1 steel in [32].
Looking more closely on numerical values for the

diffusion coefficient, below-stated considerations were taken:
the partial sputter yields (see figure 8c) are approximately constant at 10 % of the experimental fluence. They get close to steady-state and we can thus extrapolate to higher fluencies and choose parameters to match 10 % of the experimental results with modelling results for a fluence of $1 * 10^{25}$ ions/m^2. Since the partial yields have not entirely approached the steady-state, especially for Cr, values extrapolated to 100 % stay below the reference values for WCrY. The surface recession is approximately linear when W partial sputtering dominates (see figure 8c for the evolution of partial sputter yields), except for the first fluence steps. Consequently, simulation results for surface recession and indirectly obtained mass loss are extrapolated based on the last simulated fluence steps. Here the change in partial sputter yields between subsequent fluence steps becomes convergently small. Neglecting the influence of D retention, the Cr-diffusion in WCrY, $D_{Cr,WCrY}$, is likely greater than $5 * 10^{-18}$ m^2/s and situated within the range of 2 to $3 * 10^{-17}$ m^2/s as indicated in blue in figure 8a. Yet, if D retention and diffusion is considered within the model for W and WCrY the Cr diffusion coefficient has to be set to $5 * 10^{-18}$ m^2/s in order to match experimental results, besides increasing the oxygen plasma content slightly as mentioned above. In [33] it is stated that the sputter yield decreases with increased surface roughness. In [7] it was found that the initial surface roughness of about 30 nm is slightly increased for all samples by up to 20 %. Since there is no difference in the trend for W and WCrY, this effect influences a model parameter which effects the erosion of W and WCrY in the same way, e.g. rather the oxygen content and not the diffusion coefficient. From comparing the XPS-profiles of W and Cr in figure 4 to the profiles of 8c it is concluded that the diffusion coefficient is likely of the order of $1 * 10^{-17}$ m^2/s.

VII. Summary and Outlook

In conclusion one-dimensional SDTrimSP simulations including the effect of Cr-diffusion contribute to an improved understanding of the influence of various effects on the erosion of pure W and WCrY samples during plasma exposure. Reproducing the difference in volumetric and mass loss of W and WCrY samples is not possible without diffusion. Moreover, oxygen content of the D plasma and D retention within exposed samples needs to be taken into account. W and Cr-profiles obtained by XPS-analysis resemble well the target composition calculated by SDTrimSP with Cr-diffusion in the range of about $1 * 10^{-17}$ m^2/s. Further, assuming a plasma oxygen content of about 0.29 % as well as a maximal D concentration of 0.02 % in the target, both modelled surface recession and mass loss of W and WCrY match experimental results within the measurement uncertainties. For the understanding influence of e.g. surface roughness the one-dimensional model is not appropriate. SEM-pictures and analysis of the samples surface morphology and composition point to the extension of the one-dimensional model to two-dimensional SDTrimSP [34] simulations. An example of the application of 2D SDTrimSP is reported in [35]. The characteristic surface structure of the smart alloys samples due to preferential sputtering by Y and Cr cannot be rendered in one dimension.
For the modelling results presented, the value of the diffusion coefficent is valid for the temperature during the conducted plasma experiment. As the temperature of the first wall of future fusion devices such as DEMO could differ from the estimated temperatures of around 600 to 700 °C or fluctuate, it is important to consider the influence of different temperature ranges on possible processes within the wall material. Reaching temperatures of about 1000 °C will lead to both W- and Cr-oxidation as disccussed in section ii. The latter subsequently leads to enhanced Cr erosion due to the elevated sputter yields of the oxide. According to [8] the damage of PFCs due to increased heat loads during

disruptions as compared to regular operation is of great concern for DEMO. A higher temperature can lead to enhanced Cr-transport towards the surface resulting in increased erosion yields and eventually in an increased impurity concentration at the plasma edge. A similar observation on the effect of higher temperatures for the FeW system is explained in [20]: high-Cr mobility suppresses build up of gradients and therefore W enrichment. To investigate the temperature-dependence of the W surface enrichment, plasma exposure of samples cooled to much lower temperatures than in the here described experiment in PSI-2 is envisaged. Further, variation of the ion flux during plasma exposure would be useful to examine the flux dependence of W surface enrichment and erosion yields. The Cr-transport due to diffusion towards the surface and the sputtering of Cr from the surface by the incoming plasma ion flux are two counteracting processes: whereas the Cr-sputtering removes Cr atoms from the subsurface layers of the target, the Cr-diffusion towards the surface counteracts the build-up of a gradient in Cr-concentration. There may exist a flux threshold for a certain temperature above which W enrichment is suppressed. Better knowledge of the activation energy Q_a for Cr-diffusion in the WCrY-system would help investigating the temperature dependence, yet this requires additional designated experiments and models.

For a material to be used as DEMO first wall material additional effects have to be considered and are outlined below: neutron irradiation with energies up to 14 MeV puts additional loads on first wall materials. Synergistic effects of transmutation elements of W and irradiation induced compositional changes on the material properties of W are complex and need to be considered for fusion operation [36]. For W-alloys impacting neutrons can effect the different alloying elements in diverse ways. A good understanding of irradiation-induced segregation to grain boundaries of alloying and impurity elements is important also regarding mechanical properties of the material [37]. Especially Cr-segregation to the surface, contributing to the thermally activated diffusion, could, besides mechanical properties, effect the sputtering and oxidation performance of smart alloys. Investigating the effect of neutron irradiation onto the WCrY-system is a subject of future studies.

Besides neutrons, the DT-reaction creates He ions. Once these escape the plasma they can lead to the degradation of the mechanical properties and structural strength of PFCs [38]. For alloys such as WCrY additional effects could be induced by He bombardment. Higher sputter yields as compared to the lighter fuel ions D and T potentially suppress the evolution of a W-enriched layer and further contribute to enhanced Cr-diffusion.

To solve the divertor power exhaust problem in DEMO the fraction of loss power radiated from the main chamber, the SOL and the divertor region seeding impurities are needed [9]. Connected to the usage of different impurity species at different locations in the reactor the gross and net erosion of PFCs at different locations has to be assessed. Here again for the smart alloys higher sputter yields of e.g. Ar (see table 3), Kr and Xe as compared to D and T may prevent the build-up of a sufficiently thick W-enriched layer. Enhanced Cr sputtering may disqualify smart alloys as first wall components. On the other side impurity sputtering as well as CX neutrals and self-sputtering are certainly a threat also to pure W wall components.

In future studies spectroscopic measurements during plasma exposure of alloys will help investigating the evolution of sputtering, deposition and impurity generation for WCrY in comparison to pure W.

Acknowledgements

This work has been carried out within the framework of the EUROfusion Consortium and has received funding from the Euratom research and training programme 2014-2018 under grant agreement No

633053. The views and opinions expressed herein do not necessarily reflect those of the European Commission.
The research benefited from a grant of the European Commission through the Erasmus Mundus International Doctoral College in Fusion Science and Engineering (FUSION-DC).

References

[1] Ch. Linsmeier, M. Rieth, et al. Development of advanced high heat flux and plasma-facing materials. *Nuclear Fusion*, 57(9):092007, 2017.

[2] J. W. Coenen, S. Antusch, et al. Materials for DEMO and reactor applications—boundary conditions and new concepts. *Physica Scripta*, T167:014002, 2016.

[3] D. Maisonnier, I. Cook, et al. The European power plant conceptual study. *Fusion Engineering and Design*, 75-79:1173–1179, 2005.

[4] T. Wegener, F. Klein, et al. Development of yttrium-containing self-passivating tungsten alloys for future fusion power plants. *Nuclear Materials and Energy*, 9:394–398, 2016.

[5] O. Guillon, J. Gonzalez-Julian, et al. Field-Assisted Sintering Technology/Spark Plasma Sintering: Mechanisms, Materials, and Technology Developments. *Advanced Engineering Materials*, 16(7):830–849, 2014.

[6] A. Litnovsky, T. Wegener, et al. New oxidation-resistant tungsten alloys for use in the nuclear fusion reactors. *Physica Scripta*, T170:014012, 2017.

[7] J. Schmitz, A. Litnovsky, et al. WCrY smart alloys as advanced plasma-facing materials – Exposure to steady-state pure deuterium plasmas in PSI-2. *Nuclear Materials and Energy*, 2018.

[8] R. Wenninger, R. Albanese, et al. The DEMO wall load challenge. *Nuclear Fusion*, 57(4):046002, 2017.

[9] R. Wenninger, R. Kembleton, et al. The physics and technology basis entering European system code studies for DEMO. *Nuclear Fusion*, 57(1):016011, 2017.

[10] J. Roth, E. Tsitrone, et al. Recent analysis of key plasma wall interactions issues for ITER. *Journal of Nuclear Materials*, 390-391:1–9, 2009.

[11] M. Z. Tokar. An assessment for the erosion rate of DEMO first wall. *Nuclear Fusion*, 58(1):016016, 2018.

[12] M. Beckers, W. Biel, et al. Investigations of the first-wall erosion of DEMO with the CELLSOR code. *Nuclear Materials and Energy*, 12:1163–1170, 2017.

[13] K. Schmid, K. Krieger, et al. DIVIMP modeling of tungsten impurity transport in ITER. *Journal of Nuclear Materials*, 363-365:674–679, 2007.

[14] A. Kreter, C. Brandt, et al. Linear Plasma Device PSI-2 for Plasma-Material Interaction Studies. *Fusion Science and Technology*, 68(1):8–14, 2015.

[15] Y. Igitkhanov, B. Bazylev, et al. Design Strategy for the PFC in DEMO Reactor (KIT Scientific Reports ; 7637).

[16] W. Eckstein. *Computer Simulation of Ion-Solid Interactions*, volume 10 of *Springer Series in Materials Science*. Springer, Berlin and Heidelberg, 1991.

[17] A. Mutzke and R. Schneider. SDTrimSP Version 5.07: IPP-Report 12/8. 2011.

[18] W. Eckstein. Sputtered Energy Coefficient and Sputtering Yield: IPP-Report 17/29. 2011.

[19] H. Mehrer, editor. *Diffusion in Solids: Fundamentals, Methods, Materials, Diffusion-Controlled*

Processes, volume 155 of *Springer Series in Solid-State Sciences*. Springer-Verlag GmbH, Berlin Heidelberg, 2007.

[20] U. von Toussaint, A. Mutzke, et al. Simulation of coupled sputter-diffusion effects. *Physica Scripta*, T167:014023, 2016.

[21] K. Sugiyama, K. Schmid, et al. Sputtering of iron, chromium and tungsten by energetic deuterium ion bombardment. *Nuclear Materials and Energy*, 8:1–7, 2016.

[22] R. Behrisch and W. Eckstein, editors. *Sputtering by Particle Bombardment: Experiments and Computer Calculations from Threshold to MeV Energies*, volume 110 of *Topics in Applied Physics*. Springer-Verlag GmbH, Berlin Heidelberg, 2007.

[23] X. Yang and A. Hassanein. Atomic scale calculations of tungsten surface binding energy and beryllium-induced tungsten sputtering. *Applied Surface Science*, 293:187–190, 2014.

[24] Y. Hirooka, M. Bourham, et al. Evaluation of tungsten as a plasma-facing material for steady state magnetic fusion devices. *Journal of Nuclear Materials*, 196-198:149–158, 1992.

[25] J. Roth and K. Schmid. Hydrogen in tungsten as plasma-facing material. *Physica Scripta*, T145:014031, 2011.

[26] C. N. Taylor, M. Shimada, et al. Deuterium retention and blistering in tungsten foils. *Nuclear Materials and Energy*, 12:689–693, 2017.

[27] Y. Zayachuk, M.H.J. 't Hoen, et al. Deuterium retention in tungsten and tungsten–tantalum alloys exposed to high-flux deuterium plasmas. *Nuclear Fusion*, 52(10):103021, 2012.

[28] K. Schmid, V. Rieger, et al. Comparison of hydrogen retention in W and W/Ta alloys. *Journal of Nuclear Materials*, 426(1-3):247–253, 2012.

[29] M.I Guseva, A.L Suvorov, et al. Sputtering of beryllium, tungsten, tungsten oxide and mixed W–C layers by deuterium ions in the near-threshold energy range. *Journal of Nuclear Materials*, 266-269:222–227, 1999.

[30] J. Roth, J. Bohdansky, et al. *Data on low energy light ion sputtering: Report IPP 9/26*. Max-Planck-Inst. für Plasmaphysik, 1979.

[31] A. Eksaeva, E. Marenkov, et al. ERO modelling of tungsten erosion in the linear plasma device PSI-2. *Nuclear Materials and Energy*, 12:253–260, 2017.

[32] L. Qiao, P. Wang, et al. Erosion and deuterium retention of CLF-1 steel exposed to deuterium plasma. *Physica Scripta*, T170:014025, 2017.

[33] Y. Li, Y. Yang, et al. Ion radiation albedo effect: Influence of surface roughness on ion implantation and sputtering of materials. *Nuclear Fusion*, 57(1):016038, 2017.

[34] A. Mutzke, R. Schneider, et al. SDTrimSP-2D: Simulation of Particles Bombarding on a Two Dimensional Target - Version 2.0, Report IPP 12/11, Max-Planck-Institut für Plasmaphysik. 2013.

[35] U. von Toussaint and A. Mutzke. Fluence dependent changes of erosion yields and surface morphology of the iron-tungsten model system: SDTrimSP-2D simulation studies. *Nuclear Materials and Energy*, 12:318–322, 2017.

[36] A. Hasegawa, M. Fukuda, et al. Neutron irradiation effects on the microstructural development of tungsten and tungsten alloys. *Journal of Nuclear Materials*, 471:175–183, 2016.

[37] R. G. Faulkner, S. Song, et al. A model describing neutron irradiation-induced segregation to grain boundaries in dilute alloys. *Metallurgical and Materials Transactions A*, 27(11):3381–3390, 1996.

[38] Y. You, X. Kong, et al. Bubble growth from clustered hydrogen and helium atoms in tungsten under a fusion environment. *Nuclear Fusion*, 57(1):016006, 2017.